MOSAIC: a new wavefront metrology

Christopher N. Anderson[a] and Patrick P. Naulleau[b]

[a]Applied Science & Technology Graduate Group, University of California, Berkeley
Berkeley, CA 94720, USA;
[b]Center for X-ray Optics, Lawrence Berkeley National Laboratory
1 Cyclotron Road, Berkeley, CA 94720, USA

ABSTRACT

MOSAIC is a new wavefront metrology that enables complete wavefront characterization from print or aerial image based measurements. Here we describe MOSAIC and verify its utility with a model-based proof of principle.

Keywords: MOSAIC, aberration, wavefront, curvature, metrology, coherence, EUV

1. MOTIVATION

The manufacturing of high performance semiconductors requires routine monitoring of aberrations in exposure tool optics to ensure that diffraction-limited imaging remains the status quo and optical proximity correction strategies can be maintained. There are currently several metrologies devoted to this task.

One metrology in widespread use today is an integrated lateral shearing interferometer (LSI) developed by ASML branded with the name ILIAS^{TM}.[1] There are also a handful of print-based tests in use that enable the quantification of specific aberrations, i.e., astigmatism, spherical error, or coma by imaging engineered mask features. Examples known to the authors are through-focus patterning of phase dots by Dirsken et. al,[2] patterning of Zernike Fourier transform targets by Robins et. al.,[3] and patterning of coma targets by Nomura et. al,[4] all of which require the ability to pattern at the diffraction limit of the imaging optic. Finally, there is another class of print-based tests that use through focus patterning of vertical, horizontal, and oblique grating patterns to quantify astigmatism[5,6] and spherical error.[7]

As the industry progresses towards EUV lithography, integrated metrologies become increasingly difficult to implement. Moreover, print-based methods relying on diffraction-limited resist performance are hampered by the realities of resist limitations. Through-focus print-based techniques, however, have the ability to bypass resist limitations. Here we present a new wavefront metrology technique, MOSIAC (metrology of optical system aberrations by incoherent curvature sensing), which is a generalization of previously described through focus methods and enables complete* wavefront recovery from print or aerial image based measurements.

While the above discussion has been centralized to the topic of lithography (the original motivation for our work), we would would like to point out that MOSAIC is applicable to the broader context of all optical systems requiring routine wavefront characterization where it is impractical to remove the optics from the tool assembly for testing.

2. MOSAIC

2.1 Goals

MOSAIC was designed with several goals in mind: (1) complete wavefront characterization, (2) simple integration into lithographic tools, (3) scalable to any numerical aperture (NA), and (4) at wavelength. MOSAIC, as you will see, satisfies all of the above criteria.

Further author information: (Send correspondence to C.N.A.)
C.N.A: E-mail: cnanderson@berkeley.edu, Telephone: 1 510 486 5288
P.P.N.: E-mail: pnaulleau@lbl.gov, Telephone: 1 510 486 4529

*Up to the two tilt Zernike temrs, $Z = \rho\cos\theta$ and $Z = \rho\sin\theta$

2.2 Description

When an optical system is perfect, ray bundles emerging from different localized regions of the optic come to focus in the same plane (Figure 1 left). When aberrations are present, the same ray bundles focus in different longitudinal planes (Figure 1 right). The focus shift of a particular ray bundle is determined by the aberrations at the location the ray bundle emerges from the part.

The goal of MOSAIC is to map out the plane of best focus across the pupil of an imaging lens. From these data, the curvature (second derivative) of the aberration can be obtained and subsequently used to obtain the aberration itself.

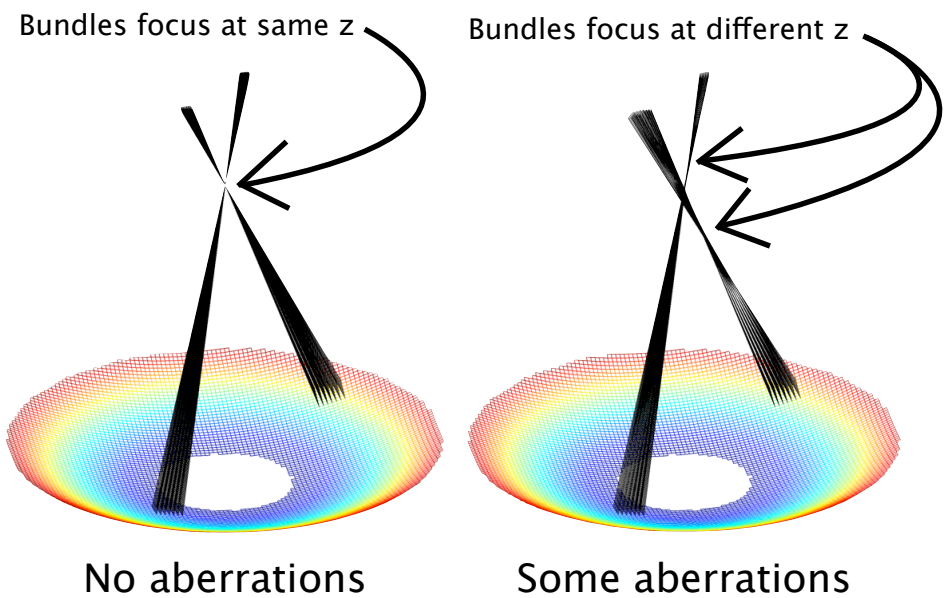

Figure 1. Left: ray bundles emerging from a perfect spherical wave come to focus in the same z plane. Right: ray bundles emerging from an aberrated spherical wave come to focus in different z planes.

2.3 The math

Consider the electric field of a plane wave: $E(\mathbf{r}) = \exp\left(i\frac{2\pi}{\lambda}\phi(\mathbf{r})\right)$ where $\phi(\mathbf{r}) = \mathbf{v}\cdot\mathbf{r}$ and $\mathbf{v} = \alpha\hat{\mathbf{x}} + \beta\hat{\mathbf{y}} + \gamma\hat{\mathbf{z}}$ is a unit vector ($\alpha^2 + \beta^2 + \gamma^2 = 1$) indicating the propagation direction. As shown below, α, β, and γ are the direction cosines of $\mathbf{v}$.

$$\alpha = \frac{\mathbf{v}\cdot\hat{\mathbf{x}}}{|\mathbf{v}|}$$
$$\beta = \frac{\mathbf{v}\cdot\hat{\mathbf{y}}}{|\mathbf{v}|}$$
$$\gamma = \frac{\mathbf{v}\cdot\hat{\mathbf{z}}}{|\mathbf{v}|}$$

When a geometrical ray propagates a distance d in the direction of $\mathbf{v}$, its x, y, and z coordinates change by dα, dβ, and dγ, respectively. Therefore, tracking the x and y coordinates of a ray as it's z coordinate changes is easy:

$$x(z) = x_0 - \frac{z\alpha}{\gamma} = x_0 - \frac{z\alpha}{\sqrt{1-\alpha^2-\beta^2}}$$
$$y(z) = y_0 - \frac{z\beta}{\gamma} = y_0 - \frac{z\beta}{\sqrt{1-\alpha^2-\beta^2}}$$

where $(x_0,\, y_0)$ is the $(x,\, y)$ point of the ray in the initial z plane. For plane waves, it is obvious that the direction cosines α and β are the x and y derivatives of $\phi(\mathbf{r})$, respectively. In the general case, the x and y derivatives of $\phi(\mathbf{r})$ still give the direction cosines, however they are *local* direction cosines, and vary with $(x_0,\, y_0)$. Below we show a general version of the x tracking equation using the derivative notation $f_x = \frac{\partial f}{\partial x}$.

$$x(z) = x_0 - z \left. \frac{\phi_x}{\sqrt{1-\phi_x^2-\phi_y^2}} \right|_{(x_0,y_0)} \tag{1}$$

Now consider a second geometrical ray, this time leaving the initial z plane from the incrementally shifted x position: $(x_0+\delta,\, y_0)$. The x position of this second ray is given by:

$$x(z) = x_0 + \delta - z \left. \frac{\phi_x}{\sqrt{1-\phi_x^2-\phi_y^2}} \right|_{(x_0+\delta,y_0)} \tag{2}$$

When the wavefront is spherical, or close to it, these geometrical rays eventually cross (focus) in x. By equating Eq. 1 and Eq. 2 we can determine the z plane where this occurs (a function of δ). By taking the limit as δ goes to zero we obtain a derivative:

$$\frac{1}{z} = \frac{\partial}{\partial x}\left(\frac{\phi_x}{\sqrt{1-\phi_x^2-\phi_y^2}}\right) \tag{3}$$

After the derivative is carried out, we obtain an equation for the second derivative (curvature) of ϕ, which, in essence, is the heart of MOSAIC:

$$\phi_{xx} = \frac{\frac{(1-\phi_x^2-\phi_y^2)^{3/2}}{z} - \phi_x\phi_y\phi_{xy}}{1-\phi_y^2} \tag{4}$$

To recap, we've derived Eq. 4 by: (1) tracing two rays that left an almost spherical wavefront from neighboring locations $(x_0,\, y_0)$ and $(x_0+\delta,\, y_0)$, (2) finding the z plane where the two rays cross in x, and (3) taking the limit of infinitesimally small δ. The outcome is a link between the x-crossing plane for a $(x_0,\, y_0)$ point of origin and the second x derivative of the wavefront at that point.[†]

2.4 Putting the math to work

Eq. 4 implies that a-priori knowledge of ϕ_x, ϕ_y, and ϕ_{xy} are required to extract ϕ_{xx}; however, ϕ_x, ϕ_y, and ϕ_{xy} of the base sphere are sufficient. Curvature data are obtained through Eq. 4 by imaging features that probe local regions $(x_0,\, y_0)$ of the optic and measuring how focus varies with $(x_0,\, y_0)$. Once ϕ_{xx} and ϕ_{yy} are sampled through the pupil, the second x and y derivatives of the base sphere can be removed, revealing the second x and y derivatives of the aberration. Finally, a least squares algorithm can be used to recover the underlying aberration from its second derivatives[‡]

[†]It is trivial to write the analogue of Eq. 4 for focus in the y direction, or any general direction

[‡]Up to the two tilt Zernike temrs, $Z = \rho\cos\theta$ and $Z = \rho\sin\theta$

2.5 Imaging while probing a local part of the lens

MOSAIC requires a small illumination coherence factor, i.e., $\sigma < 0.1$ monopole. Also, the imaged object must have large enough structure that its coherent diffraction pattern occupies a confined region of the pupil. In addition, the probe point (x_0, y_0) needs to be varied by either manually steering the illumination to different parts of the pupil in different exposures, or by utilizing a holographic mask that can probe many different parts of the pupil simultaneously, as shown in Figure 2.

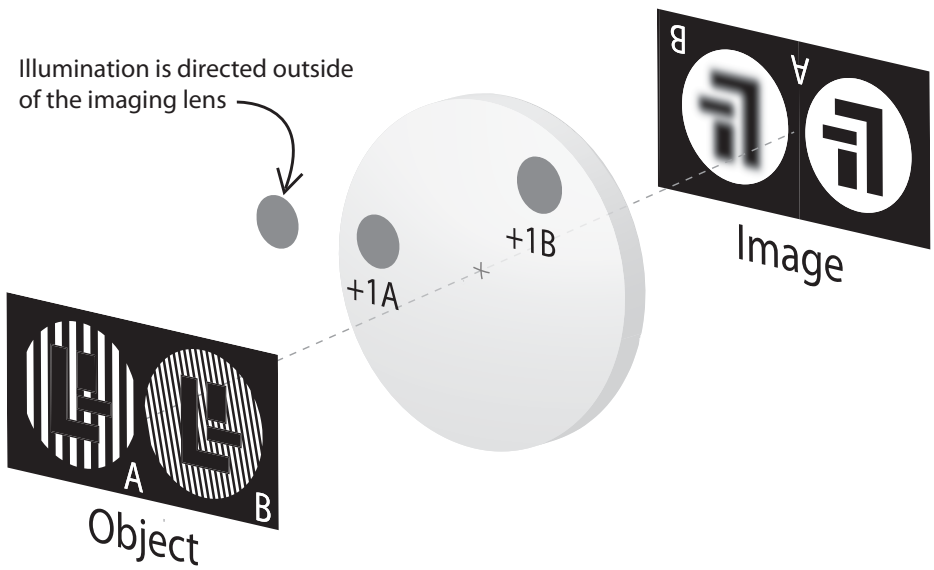

Figure 2. The holographic mask contains a test feature encoded on two different spatial carriers A and B. Off-axis coherent illumination steers the zero order (undiffracted) light outside the pupil. The +1 order diffracted light from carriers A and B (containing the test feature) probe the optic at different locations to form images of the test features in the image plane. When the optic is aberrated, each probe region may have a different focal plane. We illustrate this by showing feature A in focus and feature B out of focus.

2.6 A "catch-22?"

By design, MOSAIC requires finding focus in a regime where only a small localized region of the optic is probed as the image is formed. Therefore, the depth of focus of any given aerial image will be relatively large. Indeed, finding focus will be challenging, but not impossible. For example, employing sinusoidal phase shifting masks that eliminate the zeroth diffraction order make it possible to achieve frequency doubling in the aerial image, halving the DOF without increasing the probe area. In addition, lithographic implementations can employ resists with a large intrinsic blur and low chemical contrast to increase patterning sensitivity to changes in aerial image contrast.

2.7 Model-based proof of principle

We have modeled a MOSAIC experiment at the SEMATECH Berkeley EUV microfield exposure tool (MET) using commercial aerial image software. The Berkeley MET is a 0.3 NA, 5x reduction system with a $\sigma = 0.3$ central obscuration and an illuminator supporting fully customizable pupil fills.[8] Using an object with transmittance $t(x) = \sin(2\pi f x)$ and $f^{-1} = 400$ nm, we've suppressed the zeroth diffraction order to produce 100 nm features in the aerial image while probing only a $\sigma = 0.22$-wide (full width) area of the optic (see Figure 3). As shown in Figure 4 (left), we probe a 12 x 24, $\sigma = 0.45$ - 0.85 polar grid surrounding the MET's central obscuration[§]. The maximum sampled radial position is set so that the furthest probing diffraction order of the

[§]This is overkill. A real experiment would only sample enough points to recover the spatial frequency content of the aberration, i.e., a 3 x 12 grid

object is just collected by the lens. We model monopole illumination with a coherence factor of $\sigma = 0.08$. The plane of best focus is defined at the plane with the highest aerial image contrast, which peaks at ≈ 1 (at focus) and drops to 0.8 at the extremes of the 3 μm focus range we test. The experiment is repeated twice, once in a reference coordinate system and once in 45-degree rotated system¶. Hence we capture both astigmatism Zernikes and two independent measurements of all other Zernike coefficients.

Figure 4 (right) shows the "programmed" x-focus vs. probe map (solid lines) computed using an inverted version of Eq. 4 with known derivatives of the wavefront aberrations and the "recovered" x-focus vs. probe map (circles) computed from Eq. 4 and modeled aerial images. Figure 5 shows the programmed and recovered wavefront aberrations. The results are in good agreement over the full pupil (σ = 0.3 - 1.0) despite the limited range (σ = 0.45 - 0.85) of the MOSAIC recovery. The RMS error in the recovered wavefront is 28 pm over a σ = 0.35 - 0.95 domain, corresponding to a 4.2 percent RMS error.

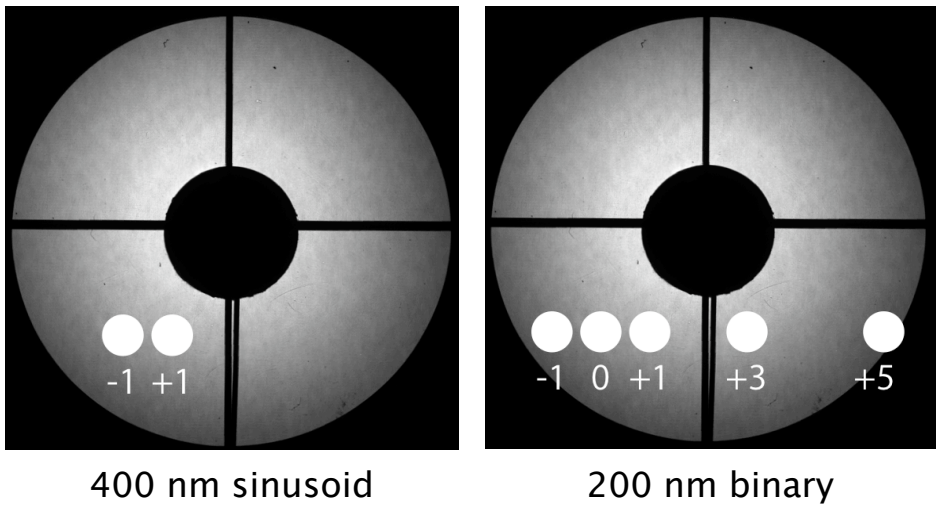

Figure 3. Left: diffraction pattern in MET pupil from a 400 nm sinusoidal grating (DC suppressed) with $\sigma = 0.08$ off-axis monopole illumination. Right: for reference, we show the diffraction pattern from a conventional 200 nm period binary grating with the same illumination.

¶We measure horizontal and vertical focus in the reference system and + 45 degree and -45 degree focus in the rotated system

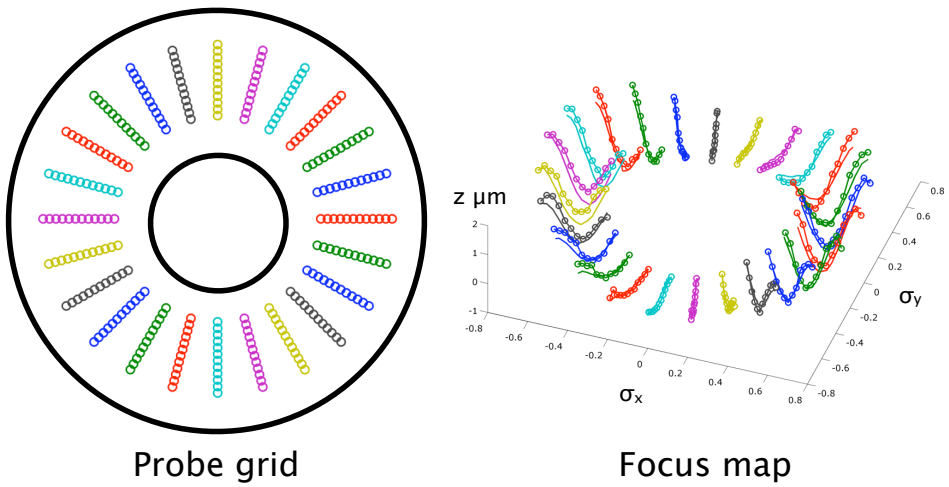

Figure 4. Left: 12 x 24, σ = 0.45 - 85 polar probe grid surrounding the σ = 0.3 central stop. Right: "programmed" x-focus vs. probe map (solid lines) vs. "measured" x-focus vs. probe map (circles).

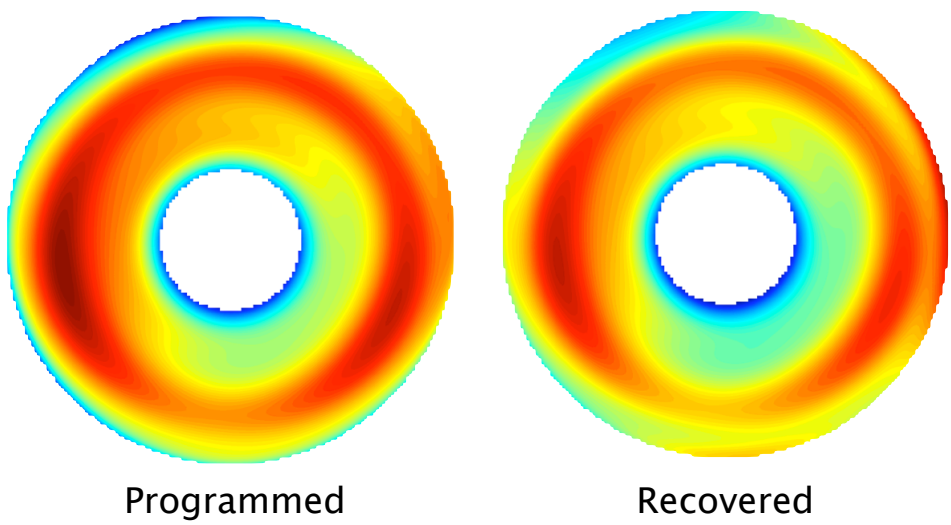

Figure 5. Left: programmed aberrations of the SEMATECH Berkeley MET pupil. Right: recovered aberrations of the full pupil ($\sigma = 0.3 - 1.0$) using MOSAIC with a σ = 0.45 - 0.85 probe domain.

3. SUMMARY

MOSAIC is an at-wavelength wavefront metrology that enables complete wavefront recovery from aerial image or print based measurements. It is based on imaging features that probe local regions of the optic and monitoring how focus varies as a function of the probe point. A model-based proof of principle assuming the aberrations of the SEMATECH Berkeley MET has been completed. The error in the MOSAIC recovery is 4.2 percent RMS over a σ = 0.35 - 0.95 subset of the MET's centrally-obscured pupil.

4. ACKNOWLEDGEMENTS

The authors are grateful for support from the NSF EUV Engineering Research Center. This work was supported by the Director, Office of Science, of the U.S. Department of Energy under Contract No. DE-AC02-05CH11231.

REFERENCES

1. M. Van De Kerkhof, W. De Boeij, H. Kok, M. Silova, J. Baselmans, and M. Hemerik. Full optical column characterization of duv lithographic projection optics. *Proc. of SPIE*, 5377:1960–1970, 2004.
2. P. Dirksen, C. Juffermans, R. Pellens, M. Maenhoudt, and P. De Bisschop. Novel aberration monitor for optical lithography. *Proc. of SPIE*, 3679:77–86, 2003.
3. G. Robins, K. Adam, and A. Neureuther. Measuring optical image aberrations with pattern and probe based targets. *JVST B*, 20(1):338–343, 2002.
4. Hiroshi Nomura and Takashi Sato. Techniques for measuring aberrations in lenses used in photolithography with printed patterns. *Applied Optics*, 38(13):2800–2807, 1999.
5. J. Kirk. Measurement of astigmatism in microlithography lenses. *Proc. of SPIE*, 3334:848–854, 1998.
6. Patrick Naulleau, Jason Cain, Kim Dean, and Kenneth A. Goldberg. Lithographic characterization of low-order aberrations in a 0.3-na euv microfield exposure tool. *Proc. of SPIE*, 6151:61512Z, 2006.
7. Patrick P. Naulleau, Jason P. Cain, and Kenneth A. Goldberg. Lithographic characterization of the spherical error in an extreme-ultraviolet optic by use of a programmable pupil-fill illuminator. *Applied Optics*, 45(9):1957–1963, 2006.
8. Y. Tanaka, H. Aoyama, K. Tawarayama, S. Magoshi, and H. Tanaka S Shirai. Status of euv micro-exposure capabilities at the als using the 0.3-na met optic. *Proc. of SPIE*, 5374:881–891, 2004.